



Article

Estimating the Fractional Cycle Biases for GPS Triple-Frequency Precise Point Positioning with Ambiguity Resolution Based on IGS Ultra-Rapid Predicted Orbits

Lizhong Qu ^{1,*}, Pu Zhang ¹, Changfeng Jing ¹ , Mingyi Du ¹, Jian Wang ¹, Qile Zhao ² and Juanjuan Li ³

¹ School of Geomatics and Urban Spatial Information, Beijing University of Civil Engineering and Architecture, 1 Zhanlanguan Road, Beijing 100044, China; zp@stu.bucea.edu.cn (P.Z.); jingcf@bucea.edu.cn (C.J.); dumingyi@bucea.edu.cn (M.D.); wangjian@bucea.edu.cn (J.W.)

² GNSS Research Center, Wuhan University, 129 Luoyu Road, Wuhan 430079, China; zhaoql@whu.edu.cn

³ 54th Research Institution, China Electronics Technology Group Corporation, 589 Zhongshanxi Road, Shijiazhuang 050000, China; lj-56031@163.com

* Correspondence: qulizhong@bucea.edu.cn

Abstract: We investigate the estimation of the fractional cycle biases (FCBs) for GPS triple-frequency uncombined precise point positioning (PPP) with ambiguity resolution (AR) based on the IGS ultra-rapid predicted (IGU) orbits. The impact of the IGU orbit errors on the performance of GPS triple-frequency PPP AR is also assessed. The extra-wide-lane (EWL), wide-lane (WL) and narrow-lane (NL) FCBs are generated with the single difference (SD) between satellites model using the global reference stations based on the IGU orbits. For comparison purposes, the EWL, WL and NL FCBs based on the IGS final precise (IGF) orbits are estimated. Each of the EWL, WL and NL FCBs based on IGF and IGU orbits are converted to the uncombined FCBs to implement the static and kinematic triple-frequency PPP AR. Due to the short wavelengths of NL ambiguities, the IGU orbit errors significantly impact the precision and stability of NL FCBs. An average STD of 0.033 cycles is achieved for the NL FCBs based on IGF orbits, while the value of the NL FCBs based on IGU orbits is 0.133 cycles. In contrast, the EWL and WL FCBs generated based on IGU orbits have comparable precision and stability to those generated based on IGF orbits. The use of IGU orbits results in an increased time-to-first-fix (TTFF) and lower fixing rates compared to the use of IGF orbits. Average TTFFs of 23.3 min (static) and 31.1 min (kinematic) and fixing rates of 98.1% (static) and 97.4% (kinematic) are achieved for the triple-frequency PPP AR based on IGF orbits. The average TTFFs increase to 27.0 min (static) and 37.9 min (kinematic) with fixing rates of 97.0% (static) and 96.3% (kinematic) based on the IGU orbits. The convergence times and positioning accuracy of PPP and PPP AR based on IGU orbits are slightly worse than those based on IGF orbits. Additionally, limited by the number of satellites transmitting three frequency signals, the introduction of the third frequency, L5, has a marginal impact on the performance of PPP and PPP AR. The GPS triple-frequency PPP AR performance is expected to improve with the deployment of new-generation satellites capable of transmitting the L5 signal.

Keywords: GPS triple-frequency; fractional cycle biases (FCBs); uncombined precise point positioning (PPP); ambiguity resolution (AR); IGS ultra-rapid predicted (IGU) orbits



Citation: Qu, L.; Zhang, P.; Jing, C.; Du, M.; Wang, J.; Zhao, Q.; Li, J. Estimating the Fractional Cycle Biases for GPS Triple-Frequency Precise Point Positioning with Ambiguity Resolution Based on IGS Ultra-Rapid Predicted Orbits. *Remote Sens.* **2021**, *13*, 3164. <https://doi.org/10.3390/rs13163164>

Academic Editor: Elisa Pinat

Received: 29 June 2021

Accepted: 6 August 2021

Published: 10 August 2021

Publisher's Note: MDPI stays neutral with regard to jurisdictional claims in published maps and institutional affiliations.



Copyright: © 2021 by the authors. Licensee MDPI, Basel, Switzerland. This article is an open access article distributed under the terms and conditions of the Creative Commons Attribution (CC BY) license (<https://creativecommons.org/licenses/by/4.0/>).

1. Introduction

With the modernization of GPS and GLONASS as well as the deployment completion of Galileo and BDS-3, increasing numbers of satellites are transmitting beyond two signals for positioning and location services. For multi-frequency precise point positioning (PPP), more wide-lane (WL) ambiguities with long wavelengths can be formed and fixed instantaneously [1]. This makes instantaneous decimeter to centimeter-level positioning accuracy obtainable even only by fixing the WL ambiguities for multi-frequency and multi-GNSS PPP [2]. Fast WL ambiguity resolution (AR) can also accelerate the narrow-lane

(NL) AR [3]. While multi-frequency PPP AR can significantly shorten the AR time and improve the positioning accuracy, the estimation of the fractional cycle biases (FCBs) of the multi-frequency phase ambiguities is crucial [4].

Some investigations have been conducted on the estimation of the multi-frequency FCBs and multi-frequency uncombined PPP AR. Based on the multi-GNSS final precise orbit and satellite clock error products of the German Research Centre for Geosciences (GFZ), Li et al. [5] estimated the uncombined FCBs with a unified model to implement the GPS, Galileo and BDS-2 triple-frequency PPP AR. The average convergence time was reduced by 15.6% with triple-frequency GNSS PPP AR compared to the dual-frequency GNSS PPP AR. With the multi-GNSS final precise orbit and satellite clock error products of Wuhan University, China, Geng et al. [3] generated the extra-WL (EWL), WL and NL FCBs with the single difference (SD) between satellite models to realize the combined GPS, Galileo, BDS-2 and QZSS triple-frequency cascading PPP AR. The positioning accuracy for the first 10 minutes was improved by approximately 50% from 0.23, 0.18 and 0.43 m to 0.12, 0.08 and 0.27 m for the east, north and up components, respectively. With the same products, Geng et al. [6] estimated a series of WL FCBs using an extended SD model for Galileo and BDS-3 five-frequency PPP WL AR. Instant positioning accuracies of 0.10 and 0.11 m were achieved for the east and north components, respectively, using Galileo five frequency signals, while corresponding accuracies of 0.16 and 0.23 m were achieved using BDS-3 five frequency signals. In addition, Laurichesse et al. [7] adopted the final precise orbit and satellite clock error products from the Centre National d'Etudes Spatiales (CNES), France to compute the uncombined FCBs of Galileo four-frequency signals. The combination of Galileo and GPS makes it possible for single-epoch centimeter-level PPP solutions and fast convergence to be reached within a few epochs.

Substantial progress has been achieved for the estimation of multi-frequency FCBs as well as multi-frequency PPP AR. However, the estimation of multi-frequency FCBs and multi-frequency PPP AR has been limited to the use of the IGS final precise (IGF) orbit and satellite clock error products. Since the IGF product is available with significant time delays, it would reduce the timeliness of the multi-frequency FCB estimates and multi-frequency PPP AR. The IGS ultra-rapid predicted (IGU) orbits can be used to support near real-time or real-time applications, but their quality is worse than the IGF orbits [8]. Although the satellite clock error corrections can compensate for some of the IGU orbit errors, the residual orbit errors are assimilated into raw ambiguities of PPP [9]. When the raw ambiguities are used to form the WL and NL ambiguity combinations for FCB estimates [6], the FCBs will be contaminated by the orbit's line-of-sight errors [10]. In particular, the NL FCBs derived from the NL ambiguities with a short wavelength will be affected and further affect the PPP AR performance [11].

The research on the precision and stability of FCB estimates for GPS triple-frequency uncombined PPP AR based on the IGU orbits is limited to date, and the impacts of the IGU orbit errors on the GPS triple-frequency uncombined PPP AR performance should be investigated. Therefore, we first describe in detail the method for creating FCB estimates as well as GPS triple-frequency PPP AR. Then, the test data to generate FCBs and implement the GPS triple-frequency PPP AR are illustrated. Subsequently, the precision and stability of EWL, WL and NL FCBs generated using global reference stations based on IGF and IGU orbits are compared and analyzed. Finally, the performance of GPS triple-frequency PPP AR with estimated FCBs is assessed.

2. GPS Triple-Frequency PPP AR

All the 32 GPS satellites transmit two frequencies: L1 (1575.42 MHz) and L2 (1227.60 MHz). At the time of writing, except for the new-generation BLOCK IIIA satellite G04 that is being tested in orbit, 12 BLOCK IIF satellites are capable of transmitting the third frequency: L5 (1176.45 MHz). Unlike the multi-frequency signals of Galileo and BDS-3 satellites, there exist apparent inconsistencies among the time-varying characteristics of the three frequency phase hardware delays of GPS BLOCK IIF satellites as well as BDS-2 satellites [12,13]. There-

fore, we first derive the observation equations of the GPS triple-frequency PPP considering this attribute [14]. Then, we describe the EWL, WL and NL cascading FCB estimation strategy based on the SD model [2]. The conversion formula from the EWL, WL and NL FCBs to the uncombined FCBs is also given, followed by the method for GPS triple-frequency PPP AR [5].

2.1. Basic Observation Equations

The undifferenced GPS observation equations of raw code and phase measurements can be expressed as

$$\begin{cases} P_{r,i}^j = \rho_{r,i}^j + dt_r - dt^s + m_r^j T_r + I_i^j + B_{r,i} - B_i^j + \varepsilon_{P_{r,i}^j} \\ L_{r,i}^j = \rho_{r,i}^j + dt_r - dt^s + m_r^j T_r - I_i^j + \lambda_i N_i^j + b_{r,i} - b_i^j - b_{v_i}^j + \varepsilon_{L_{r,i}^j} \end{cases} \quad (1)$$

where $P_{r,i}^j$ and $L_{r,i}^j$ are the code and phase observations, respectively, from receiver r to satellite j at frequency i ($i = 1, 2, 3$); $\rho_{r,i}^j$ is the geometric distance; dt_r and dt^s are the receiver and satellite clock errors, respectively; T_r is the zenith tropospheric delay (ZTD) with mapping functions m_r^j ; I_i^j is the slant ionospheric delay at frequency i ; c is the speed of light in vacuum, f_i is the frequency of phase i , $\lambda_i = c/f_i$ is the wavelength; N_i^j is the integer ambiguity; $B_{r,i}$ and B_i^j are the code hardware delays in the receiver and satellite, respectively; $b_{r,i}$ is the phase hardware delay in the receiver; b_i^j and $b_{v_i}^j$ denote the time-invariant and time-varying parts of the phase hardware delay in the satellite, respectively; and $\varepsilon_{P_{r,i}^j}$ and $\varepsilon_{L_{r,i}^j}$ denote the code and phase measurement noises, respectively.

Normally, the code and phase hardware delays in (1) cannot be directly estimated due to the rank deficiency [15]. To avoid the rank deficiency of the normal matrix, the code and phase hardware delays are included in other parameters. Moreover, to maintain compatibility with the precise satellite clock error corrections conventionally derived from L1 and L2 ionosphere-free (IF) combinations [16], the P1 and P2 code hardware delays in satellites as well as the time-varying parts of the L1 and L2 phase hardware delays in satellites are assimilated into the satellite clock error parameters [14]. Additionally, the P1 and P2 code hardware delays in the receiver are assimilated into the receiver clock error parameters [17]. Therefore, (1) is transformed into

$$\begin{cases} P_{r,1}^j = \rho_r^j + \tilde{dt}_r - \tilde{dt}^s + m_r^j T_r + g_{11} \tilde{I}_1^j + \tilde{\varepsilon}_{P_{r,1}^j} \\ P_{r,2}^j = \rho_r^j + \tilde{dt}_r - \tilde{dt}^s + m_r^j T_r + g_{12} \tilde{I}_1^j + \tilde{\varepsilon}_{P_{r,2}^j} \\ P_{r,3}^j = \rho_r^j + \tilde{dt}_r - \tilde{dt}^s + m_r^j T_r + g_{13} \tilde{I}_1^j + IFB_r^j + \tilde{\varepsilon}_{P_{r,3}^j} \\ L_{r,1}^j = \rho_r^j + \tilde{dt}_r - \tilde{dt}^s + m_r^j T_r - g_{11} \tilde{I}_1^j + \lambda_1 \tilde{N}_1^j + \varepsilon_{L_{r,1}^j} \\ L_{r,2}^j = \rho_r^j + \tilde{dt}_r - \tilde{dt}^s + m_r^j T_r - g_{12} \tilde{I}_1^j + \lambda_2 \tilde{N}_2^j + \varepsilon_{L_{r,2}^j} \\ L_{r,3}^j = \rho_r^j + \tilde{dt}_r - \tilde{dt}^s + m_r^j T_r - g_{13} \tilde{I}_1^j + \lambda_3 \tilde{N}_3^j + (g_{13} - 1)IFCB^j + \varepsilon_{L_{r,3}^j} \end{cases} \quad (2)$$

where

$$\left\{ \begin{array}{l} d\tilde{t}_r = dt_r + \frac{g_{12}B_{r,1} - B_{r,2}}{g_{12}-1} \\ d\tilde{t}^s = dt^s + \frac{g_{12}B_1^j - B_2^j}{g_{12}-1} + \frac{g_{12}b_{v_1}^j - b_{v_2}^j}{g_{12}-1} \\ \tilde{I}_1^j = I_1^j - \frac{DCB_{r,12} - DCB_{12}^j + b_{v_1}^j - b_{v_2}^j}{1-g_{12}} \\ \tilde{N}_1^j = N_1^j + [b_{r,1} - b_1^j - \frac{g_{12}+1}{g_{12}-1}(B_{r,1} - B_1^j) + \frac{2}{g_{12}-1}(B_{r,2} - B_2^j)]/\lambda_1 \\ \tilde{N}_2^j = N_2^j + [b_{r,2} - b_2^j - \frac{2g_{12}}{g_{12}-1}(B_{r,1} - B_1^j) + \frac{g_{12}+1}{g_{12}-1}(B_{r,2} - B_2^j)]/\lambda_2 \\ \tilde{N}_3^j = N_3^j + [b_{r,3} - b_3^j - \frac{g_{12}}{g_{12}-1}(1 + g_{23})(B_{r,1} - B_1^j) + \frac{1}{g_{12}-1}(1 + g_{13})(B_{r,2} - B_2^j)]/\lambda_3 \\ IFB_r^j = -\frac{1}{g_{12}-1}(1 - g_{23})B_{r,1} + \frac{1}{g_{12}-1}(1 - g_{13})B_{r,2} + B_{r,3} + DCB_{12}^j + \frac{1}{g_{12}-1}(1 - g_{13})DCB_{13}^j \\ IFCB^j = \left[\frac{-g_{12}}{g_{12}-1}(1 - g_{23})b_{v_1}^j - \frac{1}{g_{12}-1}(1 - g_{13})b_{v_2}^j - b_{v_3}^j \right] / (g_{13} - 1) \end{array} \right. \quad (3)$$

In (2) and (3), $g_{1i} = f_1^2/f_i^2$, $g_{23} = g_{13}/g_{12}$; $d\tilde{t}_r$ and $d\tilde{t}^s$ are the transformed receiver and satellite clock errors, respectively; \tilde{I}_1^j is the transformed slant ionospheric delay at the first frequency and $\tilde{I}_i^j = g_{1i}\tilde{I}_1^j$; \tilde{N}_i^j is the transformed float ambiguity; $DCB_{r,12}$ denotes the receiver differential code bias (DCB), defined as the difference between $B_{r,1}$ and $B_{r,2}$; and DCB_{12}^j and DCB_{13}^j denote the satellite DCBs, defined as the differences between B_1^j and B_2^j and between B_1^j and B_3^j , respectively.

In addition, an extra receiver and satellite-dependent code bias, termed the inter-frequency bias (IFB), is added for L5 code observations [17]. Moreover, satellite-dependent inter-frequency clock biases (IFCBs), defined as the differences between precise satellite clock errors estimated based on L1/L2 and L1/L5 IF combinations [18], are added for L5 phase observations [14]. Then, the new code noise $\tilde{\varepsilon}_{r,i}^{p,j}$ can be expressed as

$$\left\{ \begin{array}{l} \tilde{\varepsilon}_{r,1}^{p,j} = \varepsilon_{r,1}^{p,j} + \frac{g_{12}+1}{g_{12}-1}b_{v_1}^j - \frac{2}{g_{12}-1}b_{v_2}^j \\ \tilde{\varepsilon}_{r,2}^{p,j} = \varepsilon_{r,2}^{p,j} + \frac{2}{g_{12}-1}b_{v_1}^j - \frac{g_{12}+1}{g_{12}-1}b_{v_2}^j \\ \tilde{\varepsilon}_{r,3}^{p,j} = \varepsilon_{r,3}^{p,j} + \frac{g_{12}}{g_{12}-1}(1 + g_{23})b_{v_1}^j - \frac{1}{g_{12}-1}(1 + g_{13})b_{v_2}^j \end{array} \right. \quad (4)$$

As (4) shows, $\tilde{\varepsilon}_{r,i}^{p,j}$ absorbs the time-varying parts of the L1 and L2 phase hardware delays in satellites, the impacts of which on the positioning accuracy can be neglected due to the codes having much smaller weights than the phases.

2.2. FCBs Estimation and PPP AR

By adopting the precise satellite orbit, clock error corrections and station coordinates, GPS triple-frequency float uncombined PPP is implemented for each reference station. The float ambiguities are extracted for epoch-wise FCB estimations. Then, the float EWL ambiguity \tilde{N}_{ewl}^j , WL ambiguity \tilde{N}_{wl}^j and IF ambiguity \tilde{N}_{IF}^j are computed as

$$\left\{ \begin{array}{l} \tilde{N}_{ewl}^j = \tilde{N}_2^j - \tilde{N}_5^j = N_{ewl}^j + \tilde{b}_{r,ewl} - \tilde{b}_{ewl}^j \\ \tilde{N}_{wl}^j = \tilde{N}_1^j - \tilde{N}_2^j = N_{wl}^j + \tilde{b}_{r,wl} - \tilde{b}_{wl}^j \\ \tilde{N}_{IF}^j = \frac{g\tilde{N}_1^j - \tilde{N}_2^j}{g-1} = \tilde{N}_{nl}^j + \frac{\tilde{N}_{wl}^j}{g-1} \end{array} \right. \quad (5)$$

where $g = f_1/f_2$; N_{ewl}^j and N_{wl}^j are the integer parts of \tilde{N}_{ewl}^j and \tilde{N}_{wl}^j , respectively; $\tilde{b}_{r,ewl}$ and $\tilde{b}_{r,wl}$ are the combined fractional parts of the receiver hardware delay biases of \tilde{N}_{ewl}^j and \tilde{N}_{wl}^j , respectively; \tilde{b}_{ewl}^j and \tilde{b}_{wl}^j are the combined fractional parts of the satellite hardware delay biases of \tilde{N}_{ewl}^j and \tilde{N}_{wl}^j , respectively; and \tilde{N}_{nl}^j is the float NL ambiguity.

To eliminate the receiver hardware delay biases, the SD EWL ambiguity \tilde{N}_{ewl}^{jm} and WL ambiguity \tilde{N}_{wl}^{jm} are formed as

$$\begin{cases} \tilde{N}_{ewl}^{jm} = \tilde{N}_{ewl}^j - \tilde{N}_{ewl}^m = N_{ewl}^{jm} - \tilde{b}_{ewl}^{jm} \\ \tilde{N}_{wl}^{jm} = \tilde{N}_{wl}^j - \tilde{N}_{wl}^m = N_{wl}^{jm} - \tilde{b}_{wl}^{jm} \end{cases} \quad (6)$$

where $j = n, n-1, \dots, 2$, $m = n-1, n-2, \dots, 1$, $j > m$, n is the total satellite number; N_{ewl}^{jm} and N_{wl}^{jm} are the integer parts of \tilde{N}_{ewl}^{jm} and \tilde{N}_{wl}^{jm} , respectively; and \tilde{b}_{ewl}^{jm} and \tilde{b}_{wl}^{jm} are the combined fractional parts of \tilde{N}_{ewl}^{jm} and \tilde{N}_{wl}^{jm} , respectively.

We compute the integer parts of \tilde{N}_{ewl}^{jm} and \tilde{N}_{wl}^{jm} through a rounding operation, and the fractional parts are derived by subtracting the integer parts from \tilde{N}_{ewl}^{jm} and \tilde{N}_{wl}^{jm} , respectively. Subsequently, the SD EWL FCB \bar{b}_{ewl}^{jm} and WL FCB \bar{b}_{wl}^{jm} are calculated by averaging the fractional parts of \tilde{N}_{ewl}^{jm} and \tilde{N}_{wl}^{jm} of all reference stations, respectively,

$$\begin{cases} \bar{b}_{ewl}^{jm} = \tilde{N}_{ewl}^{jm} - [\tilde{N}_{ewl}^{jm}] \\ \bar{b}_{wl}^{jm} = \tilde{N}_{wl}^{jm} - [\tilde{N}_{wl}^{jm}] \end{cases} \quad (7)$$

where $[\cdot]$ and \cdot denote rounding and averaging operations, respectively. As long as the EWL and WL FCBs of all satellite pairs are acquired, a least-square adjustment is applied to estimate the EWL and WL FCBs (i.e., \bar{b}_{ewl}^j and \bar{b}_{wl}^j) by choosing a BLOCK IIF satellite tracked by most stations as a reference.

After fixing \tilde{N}_{wl}^{jm} by correcting \bar{b}_{wl}^{jm} with the rounding operation, the SD NL ambiguity \tilde{N}_{nl}^{jm} is obtained from the SD float IF combination ambiguity \tilde{N}_{IF}^{jm} according to

$$\begin{cases} \tilde{N}_{nl}^{jm} = \tilde{N}_{IF}^{jm} - \frac{[\tilde{N}_{wl}^{jm} - \bar{b}_{wl}^{jm}]}{g-1} = N_{nl}^{jm} - \tilde{b}_{nl}^{jm} \\ \bar{b}_{nl}^{jm} = \tilde{N}_{nl}^{jm} - [\tilde{N}_{nl}^{jm}] \end{cases} \quad (8)$$

where N_{nl}^{jm} and \tilde{b}_{nl}^{jm} are the integer and combined fractional parts of \tilde{N}_{nl}^{jm} , respectively. We compute the integer part of \tilde{N}_{nl}^{jm} through a rounding operation, and the fractional part is derived by subtracting the integer parts from \tilde{N}_{nl}^{jm} . Subsequently, the SD NL FCB \bar{b}_{nl}^{jm} is calculated by averaging the fractional parts of \tilde{N}_{nl}^{jm} of all reference stations.

Then, a least-square adjustment is applied to generate NL FCBs (i.e., \bar{b}_{nl}^j), for which the reference satellite used to estimate the EWL and WL FCBs is adopted. To decrease the impacts of the residual atmosphere delay error absorbed into the ambiguities on the estimation of FCBs, ambiguities with average multi-epoch elevations smaller than 10° are not used to form the SD ambiguities. When estimating the EWL, WL and NL FCBs, satellite pairs tracked by fewer than 5 stations are removed; furthermore, the EWL, WL and NL FCBs of satellite pairs whose residuals are larger than 0.3 cycles are rejected.

When implementing GPS dual-frequency PPP AR, Li et al. [19] estimated the uncombined FCBs from the WL FCBs \bar{b}_{wl}^j and NL FCBs \bar{b}_{nl}^j according to

$$\begin{bmatrix} \bar{b}_1^j \\ \bar{b}_2^j \end{bmatrix} = \begin{bmatrix} -\frac{1}{g-1} & 1 \\ -\frac{g}{g-1} & 1 \end{bmatrix} \begin{bmatrix} \bar{b}_{wl}^j \\ \bar{b}_{nl}^j \end{bmatrix} \quad (9)$$

where \bar{b}_1^j and \bar{b}_2^j are the FCB corrections for the L1 and L2 ambiguities of satellite j , respectively.

For GPS Block IIR and Block IIR-M satellites, we still follow (9) to estimate the uncombined FCBs. For Block IIF satellites, we estimate the uncombined FCBs from the EWL FCBs \bar{b}_{ewl}^j , WL FCBs \bar{b}_{wl}^j and NL FCBs \bar{b}_{nl}^j according to

$$\begin{bmatrix} \bar{b}_1^j \\ \bar{b}_2^j \\ \bar{b}_5^j \end{bmatrix} = \begin{bmatrix} 0 & -\frac{1}{s-1} & 1 \\ 0 & -\frac{s}{s-1} & 1 \\ -1 & -\frac{s}{s-1} & 1 \end{bmatrix} \begin{bmatrix} \bar{b}_{ewl}^j \\ \bar{b}_{wl}^j \\ \bar{b}_{nl}^j \end{bmatrix} \quad (10)$$

where \bar{b}_1^j , \bar{b}_2^j and \bar{b}_5^j are the FCB corrections for the L1, L2 and L5 ambiguities of satellite j , respectively.

As long as the uncombined FCBs are acquired, the GPS triple-frequency PPP AR is implemented. First, the float SD ambiguities \tilde{N}_i^{jp} at each frequency are formed to eliminate the receiver FCBs. The satellites with the highest average multi-epoch elevations are taken as references. Then, the SD FCBs \bar{b}_i^{jp} are constructed to correct the float SD ambiguities, which can be expressed as

$$N_i^{jp} = \tilde{N}_i^{jp} - \bar{b}_i^{jp} \quad (11)$$

where N_i^{jp} is the corrected SD ambiguity.

Due to the strong correlation among PPP ambiguities, the corrected SD ambiguities with the reconstructed variance–covariance matrix are inserted into a search strategy based on the least-square ambiguity decorrelation adjustment (LAMBDA) method [20] to search for the integer solution of SD ambiguities. The ratio test and bootstrapped success rate test [21] are used to validate the AR solution. The critical criterion of the ratio test is set to 3.0 [22], and that of the bootstrapped success rate test is selected as 0.99 [5]. In addition, the partial ambiguity resolution (PAR) method is used to choose the optimal independent set of SD ambiguities [2], and the threshold value of the minimum number of ambiguities is set to 5 to ensure high reliability [23].

2.3. Test Data Description

To assess the performance of the FCB estimates and GPS triple-frequency PPP AR based on the IGU orbits, a total of 100 uniformly distributed global reference stations capable of receiving GPS three-frequency signals from the IGS Multi-GNSS Experiment (MGEX) network were used for experiments and numerical analyses [24]. Eighty-five stations were taken as reference stations to estimate the satellite clock error corrections, IFCBs and FCBs, while the remaining 15 stations were taken as rovers to implement GPS PPP and PPP AR. The station distribution is presented in Figure 1. Data were collected over the 15 day period from DOY 112 to 126 (April 22–May 6), 2019. The sample interval of observation data is 30 s.

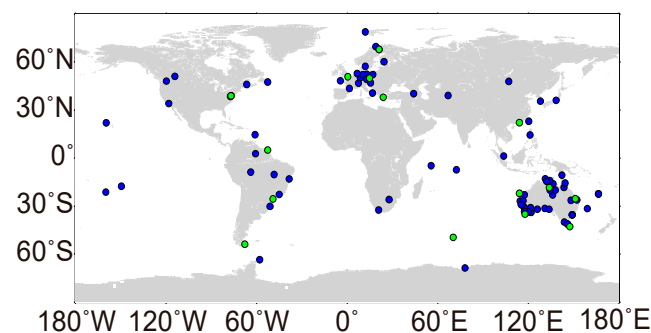


Figure 1. Station distribution used for the experiments and numerical analyses. Blue circles represent the 85 reference stations. Green circles represent the 15 rovers.

The IGS ultra-rapid orbit products were downloaded during data processing. Since the IGS ultra-rapid orbits update every 6 h with a latency of 3 h, only the parts of the predicted orbits within the predicted period from 3 to 9 h (the IGU orbits) were extracted and compared with the IGF orbits [10]. As illustrated in Figure 2, the RMSs of the differences between the IGU and IGF orbits of the along, cross and radial components of GPS satellites over the 15 day period were less than 5.0, 2.0 and 2.0 cm, respectively, and the average RMS values for these three components of all the satellites were 2.7, 1.6 and 1.0 cm, respectively. In addition, the satellite clock error corrections were estimated to compensate for the IGU orbit errors [4]. The average standard deviations (STDs) of the differences between the estimated and final satellite clock error corrections over the 15 day period were less than 4 cm, and the average STD for all the satellites was 2.1 cm. The RMSs of the user-equivalent range errors (UEREs) of GPS satellites over the 15 day period were less than 4 cm, and the average RMS for all the satellites was 2.5 cm.

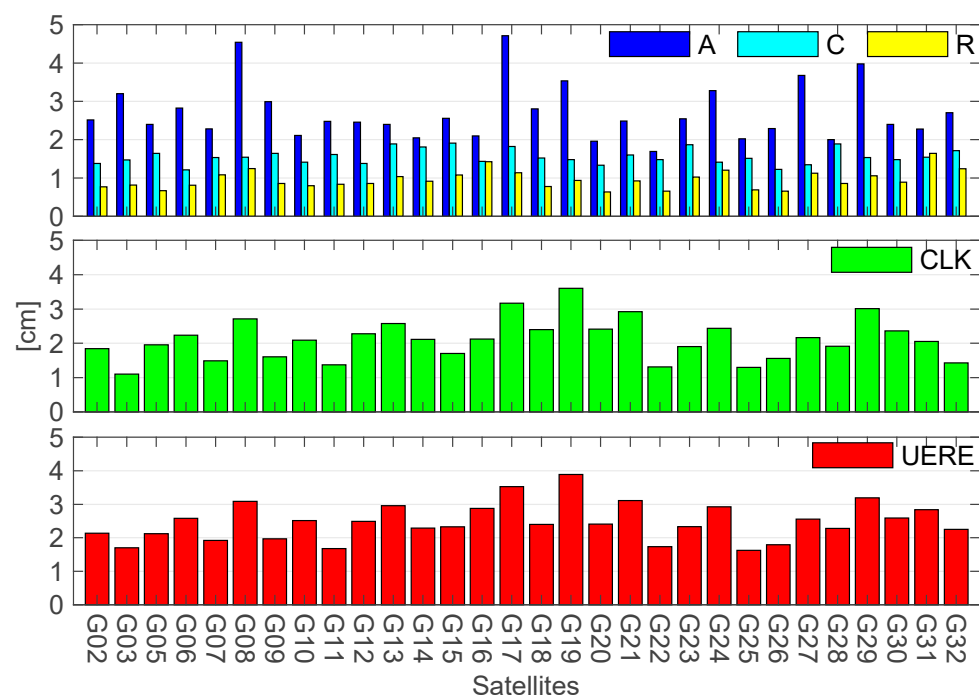


Figure 2. RMSs of the differences between the IGU and IGF orbits of along, cross and radial components (upper panel), STDs of the differences between the estimated satellite clock errors and IGF satellite clock errors (middle panel) and RMSs of the UEREs of GPS satellites (lower panel). We took G01 as the reference satellite when calculating the differences between the estimated satellite clock errors and IGF ones. Thus, the values of G01 are not shown.

The IFCBs vary cyclically from day to day with respect to the Sun–satellite–Earth geometry [12], and this variation has a substantial impact on GPS triple-frequency PPP and PPP AR [5]. Thus, the IFCBs need to be eliminated before FCB estimations and GPS triple-frequency PPP AR. To avoid introducing orbit errors into IFCB estimates, the Epoch-Differenced (ED) method based on a Geometry-Free (GF) IF combination of three frequency phases was adopted, as in Li et al. [25]. As demonstrated in Figure 3, the IFCBs were time and satellite-dependent, and the maximum 24 h variation could reach 10 cm. In addition, Figure 4 confirms that the impact of IFCBs on phase residuals is frequency-dependent. The RMSs of the L1, L2 and L5 phase residuals without IFCB corrections were 4.7, 7.7 and 8.0 mm, respectively, whereas the corresponding RMSs decreased to 3.8, 2.4 and 2.3 mm, respectively, with IFCB corrections.

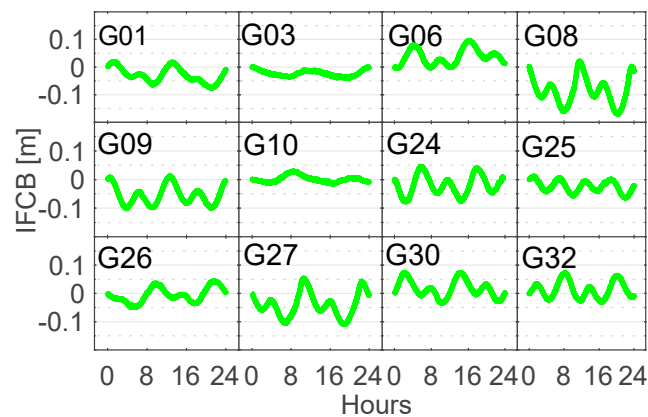


Figure 3. Time series of IFCBs on DOY 118, 2019.

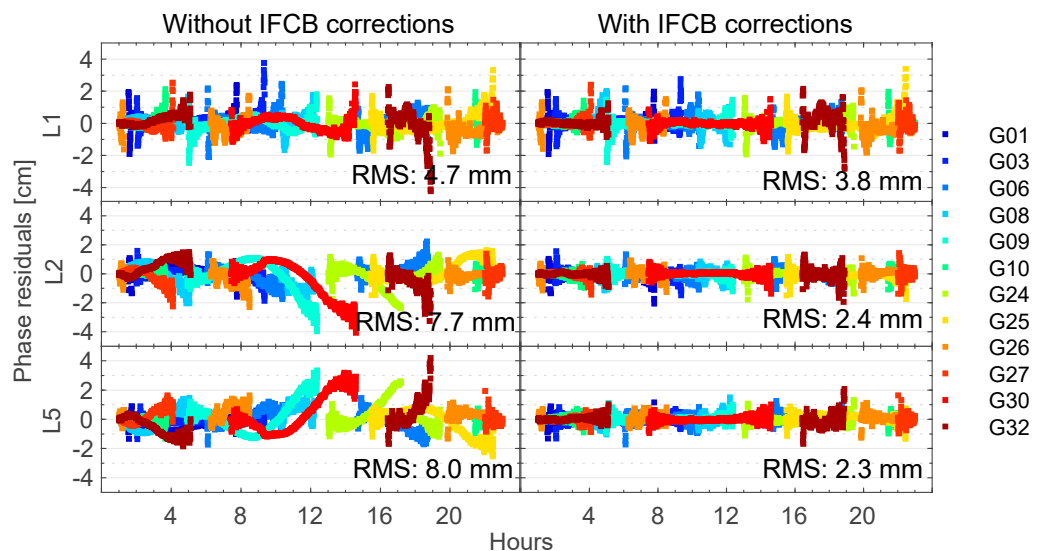


Figure 4. Phase residuals of triple-frequency PPP with and without IFCB corrections on DOY 118, 2019.

For the estimation of FCBs and for GPS triple-frequency PPP AR, the slant ionosphere delay was estimated as a random-walk process parameter. Furthermore, corrections for the satellite antenna phase center offsets (PCOs) and phase center variations (PCVs) of the L2 frequency were applied to the L5 frequency. As for the stations, the corrections of the L2 frequency were applied to the L5 frequency as the receiver antenna PCOs and PCVs of the L5 frequency were unknown. In addition, the IFBs were regarded as daily constants. However, we did not consider correcting the receiver and satellite DCBs because they are commonly assumed to be constants for several days and are capable of being entirely assimilated into other parameters; thus, the DCBs did not affect the positioning accuracy.

3. Results and Analysis

In this section, the precision and stability of the EWL, WL and NL FCBs as well as the performance of GPS triple-frequency PPP and PPP AR based on IGF and IGU orbits are investigated and compared.

3.1. FCB Results and Analysis

Figure 5 displays the time series of EWL, WL and NL FCBs generated with a 900 s interval based on IGF and IGU orbits on DOY 122, 2019. The variations in the EWL, WL and NL FCBs generated based on IGF orbits as well as the EWL and WL FCBs generated

based on IGF orbits were smaller than 0.1 cycles for every satellite in a one day period. In contrast, the variations in the NL FCBs generated based on IGF orbits were smaller than 0.2 cycles for every satellite in a one day period. Moreover, the average standard deviations (STDs) of the EWL, WL and NL FCBs based on IGF orbits over the 15 day period were 0.039, 0.046 and 0.033 cycles, respectively, while those of the EWL, WL and NL FCBs based on IGF orbits were 0.037, 0.046 and 0.133 cycles, respectively.

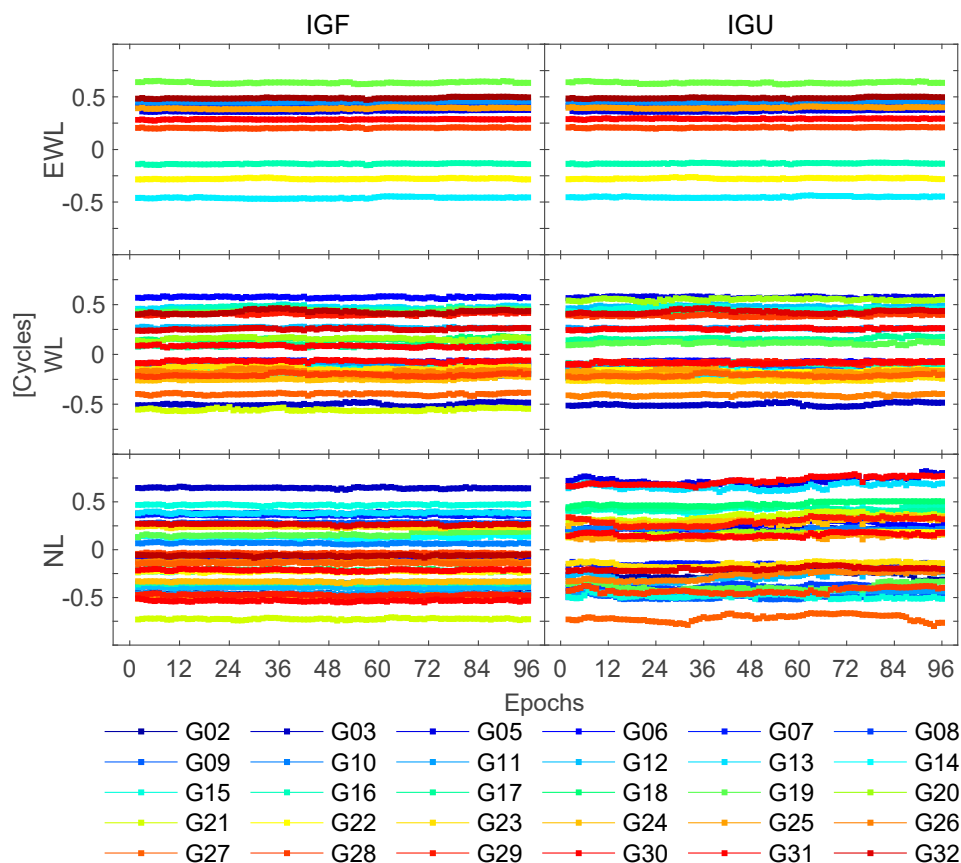


Figure 5. Time series of the EWL, WL and NL FCBs on DOY 118, 2019. G01 is the reference satellite.

Figure 6 displays the distributions of the differences between the EWL, WL and NL FCBs and their daily average values based on IGF and IGF orbits from DOY 112 to 126, 2019. The percentages of the differences between -0.15 and 0.15 cycles for the EWL, WL and NL FCBs based on IGF orbits over the 15 day period were 100.0%, 99.9% and 100.0%, respectively, while those for the EWL, WL and NL FCBs based on IGF orbits were 100.0%, 100.0% and 73.2%, respectively, indicating that the NL FCBs based on IGF orbits may contain the variation of IGF orbit errors. Moreover, the percentages of the differences between -0.25 and 0.25 cycles for the EWL, WL and NL FCBs based on IGF orbits over the 15 day period were 100.0%, 100.0% and 100.0%, respectively, while those for the EWL, WL and NL FCBs based on IGF orbits were 100.0%, 100.0% and 96.8%, respectively.

Figure 7 presents the distributions of the EWL, WL and NL FCB residuals based on IGF and IGF orbits from DOY 112 to 126, 2019. The percentages of the residuals between -0.15 and 0.15 cycles for the EWL, WL and NL FCBs based on IGF orbits over the 15 day period were 99.7%, 98.1% and 99.2%, respectively, while those for the EWL, WL and NL FCBs based on IGF orbits were 99.8%, 98.1% and 95.5%, respectively. Moreover, the percentages of the residuals between -0.25 and 0.25 cycles for the EWL, WL and NL FCBs based on IGF orbits over the 15 day period were 99.9%, 99.8% and 99.9%, respectively, while those for the EWL, WL and NL FCBs based on IGF orbits were 99.9%, 99.8% and 99.2%, respectively. In addition, the root-mean-square deviations (RMSs) of the EWL, WL and NL FCB residuals

based on IGF orbits over the 15 day period were 0.006, 0.032 and 0.025 cycles, respectively, while those of the EWL, WL and NL FCB residuals based on IGU orbits were 0.006, 0.032 and 0.040 cycles, respectively.

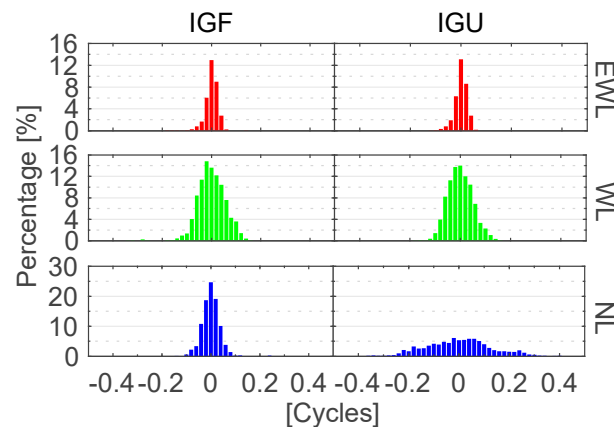


Figure 6. Distributions of the differences between the EWL, WL and NL FCBs and their daily average values from DOY 112 to 126, 2019.

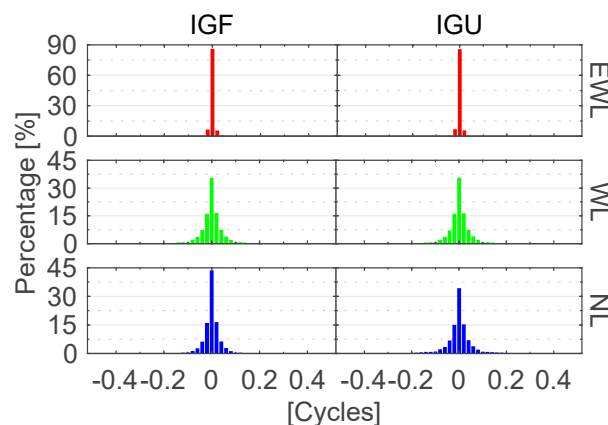


Figure 7. Distributions of the EWL, WL and NL FCB residuals from DOY 112 to 126, 2019.

Due to the high accuracy of IGF orbits, the EWL, WL and NL FCBs exhibited good numerical precision and stability. However, the average STDs of NL FCBs and the RMSs of NL FCB residuals were smaller than WL FCBs and WL FCB residuals. This may have been caused by the residual ionospheric delay errors, since they were absorbed by the raw L1 and L2 ambiguities used to estimate the WL FCBs [26]. The EWL and WL FCBs generated based on IGU orbits showed comparable performance to those generated based on IGF orbits, and the EWL FCBs performed much better in terms of numerical precision and stability than WL FCBs. This finding further illustrates that the long wavelengths of ambiguity combinations can effectively decrease the impacts of IGU orbit errors and residual ionospheric delay errors. In contrast, the NL FCBs generated based on IGU orbits exhibited the worst numerical precision and stability, which can be attributed to the short wavelength of NL ambiguities; consequently, the residual IGU orbit errors can have a significant impact on the precision and stability of NL FCBs.

3.2. PPP Results and Analysis

The PPP and PPP AR performances of the five groups of solutions based on IGF and IGU orbits are compared and analyzed: L1/L2 dual-frequency float PPP (Solution A), L1/L2/L5 triple-frequency float PPP (Solution B), dual-frequency PPP AR with fixed L1 and L2 ambiguities (Solution C), triple-frequency PPP AR with fixed L1 and L2 ambiguities but unfixed L5 ambiguities (Solution D) and triple-frequency PPP AR with fixed L1, L2

and L5 ambiguities (Solution E). First, the times to first fix (TTFFs) and fixing rates of the three groups of 24 h PPP AR solutions are evaluated. We define the TTFF as the time taken to fix the first ambiguity successfully. The fixing rate is defined as the ratio of the number of successfully fixed epochs to the total number of epochs. An epoch is successfully fixed if the ratio test, the success rate test and PAR strategy are passed.

Subsequently, the five groups of solutions are investigated in terms of their convergence time and positioning accuracy. All five groups of solutions are compared with the “ground truths”, which were derived from the average values of network solutions over 15 days. For the static solutions, the convergence time is defined as the time taken for the horizontal and vertical positioning errors to become less than 5 cm for at least 20 epochs [27]. The average RMS values of the east, north and up components of the five groups of static 1 h solutions for all rovers over 15 days are shown in Table 1. For the kinematic solutions, the corresponding metric of horizontal and vertical positioning errors used to define the convergence time is 10 cm [22]. The average RMS values of the east, north and up components of the five groups of kinematic 2 h solutions after convergence for all rovers over 15 days are shown in Table 2.

Table 1. Summary of results for static PPP and PPP AR.

| Item | TTFF (min) | | Fixing Rate (%) | | Convergence Time (min) | | | | RMS (cm) | | | | | |
|------|------------|------|-----------------|------|------------------------|----|-----|----|----------|-----|-----|-----|-----|-----|
| | IGF | IGU | IGF | IGU | IGF | | IGU | | IGF | | | IGU | | |
| | | | | | H | V | H | V | E | N | U | E | N | U |
| A | - | - | - | - | 38 | 29 | 38 | 30 | 3.0 | 1.0 | 2.8 | 3.1 | 1.0 | 2.9 |
| B | - | - | - | - | 38 | 29 | 38 | 29 | 3.2 | 1.0 | 2.7 | 3.2 | 1.0 | 2.8 |
| C | 26.1 | 30.6 | 97.9 | 96.5 | 26 | 23 | 28 | 25 | 0.4 | 0.4 | 1.5 | 0.6 | 0.6 | 1.8 |
| D | 24.7 | 29.3 | 98.0 | 96.6 | 26 | 22 | 28 | 24 | 0.5 | 0.5 | 1.6 | 0.7 | 0.6 | 1.8 |
| E | 23.3 | 27.0 | 98.1 | 97.0 | 25 | 22 | 27 | 24 | 0.5 | 0.5 | 1.6 | 0.7 | 0.6 | 1.8 |

Table 2. Summary of results for kinematic PPP and PPP AR.

| Item | TTFF (min) | | Fixing Rate (%) | | Convergence Time (min) | | | | RMS (cm) | | | | | |
|------|------------|------|-----------------|------|------------------------|----|-----|----|----------|-----|-----|-----|-----|-----|
| | IGF | IGU | IGF | IGU | IGF | | IGU | | IGF | | | IGU | | |
| | | | | | H | V | H | V | E | N | U | E | N | U |
| A | - | - | - | - | 38 | 30 | 40 | 32 | 1.3 | 1.1 | 2.8 | 1.4 | 1.2 | 3.1 |
| B | - | - | - | - | 38 | 30 | 40 | 32 | 1.3 | 1.1 | 2.8 | 1.4 | 1.2 | 3.0 |
| C | 36.0 | 43.9 | 97.0 | 95.6 | 32 | 28 | 35 | 30 | 0.7 | 0.8 | 2.4 | 0.9 | 1.1 | 2.6 |
| D | 34.6 | 42.2 | 97.1 | 95.8 | 32 | 27 | 35 | 30 | 0.7 | 0.9 | 2.4 | 0.9 | 1.0 | 2.6 |
| E | 31.1 | 37.9 | 97.4 | 96.3 | 31 | 27 | 34 | 30 | 0.7 | 0.9 | 2.4 | 0.9 | 1.0 | 2.6 |

3.2.1. Static PPP

The average TTFFs and fixing rates of the three groups of static PPP AR solutions based on IGF and IGU orbits over the 15 day period for every rover are displayed in Figure 8. The average TTFFs of 26.1 and 30.6 min were achieved for Solution C based on IGF and IGU orbits, respectively, for all the rovers. The TTFFs of Solutions C based on IGF orbits were a little larger than the values in Li et al. [5] and Hu et al. [28]. This may have been caused by the different test stations used. The TTFFs of Solution C were the longest among the three groups of PPP AR solutions. Solution D achieved average TTFFs of 24.7 and 29.3 min, respectively while the average TTFFs reached 23.3 and 27.0 min for Solution E, respectively. The TTFFs were shorter for Solutions D and E, and the fastest TTFF was achieved for Solution E. The slight improvement can be attributed to only 12 BLOCK IIF satellites capable of transmitting an L5 signal. Furthermore, the EWL ambiguities with long wavelengths could be quickly searched and fixed by introducing the third frequency, L5, in the ambiguities search stage. However, the TTFFs of Solutions E based on IGF orbits were longer than the values in Liu et al. [29], which may have been due to the satellites’ DCBs not

being corrected and more IFB parameters being estimated. In addition, due to the impact of IGU orbit errors as well as the lower precision and poorer stability of FCB estimates, the three groups of PPP AR solutions based on IGU orbits had longer TTFFs than those based on IGF orbits. The average TTFFs of the three groups of PPP AR solutions based on IGU orbits were 17.2%, 18.6% and 15.9% longer than those based on IGF orbits, respectively.

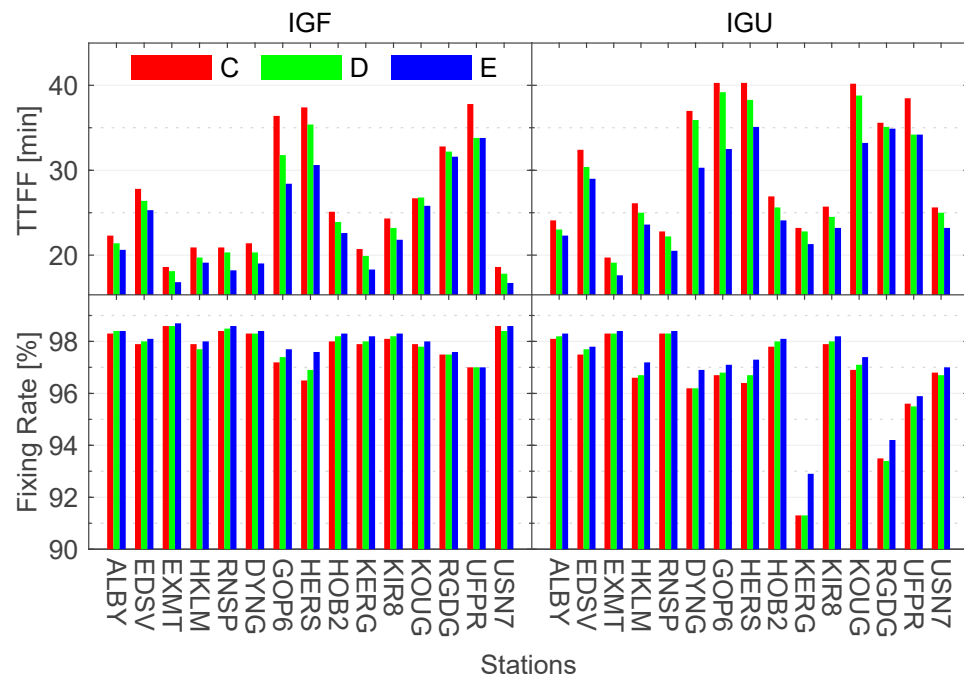


Figure 8. Average TTFFs and fixing rates of the three groups of static 24 h PPP AR solutions for every rover from DOY 112 to 126, 2019.

Average fixing rates of 97.9% and 96.5% were achieved for Solution C based on IGF and IGU orbits, respectively, for all the rovers. Solution D achieved average fixing rates of 98.0% and 96.6%, respectively, while the average fixing rates reached 98.1% and 97.0% for Solution E, respectively. The fixing rates of Solution C were the lowest among the three groups of PPP AR solutions for every rover. The fixing rates increased slightly for Solutions D and E, and the highest fixing rate was achieved for Solution E. This may have been due to the introduction of the third frequency, L5, increasing the number of candidate ambiguities, improving the rate of passing the ambiguity test. In addition, due to the longer TTFFs achieved, the three groups of PPP AR solutions based on IGU orbits had lower fixing rates than those based on IGF orbits.

Additionally, to evaluate the convergence times of five groups of static solutions based on IGF and IGU orbits, the PPP process was restarted every 2 hours. Figure 9 presents the average position errors as a function of time since the start of PPP for all 15 stations from DOY 112 to 126, 2019. A total of 2475 independent static PPP runs were performed for this analysis. Compared to static PPP, the convergence time decreased substantially, and the positioning accuracy improved greatly for static PPP AR. Furthermore, the introduction of the third frequency, L5, had a marginal impact on the convergence time of the static PPP and PPP AR. This may have been resulted from only 12 BLOCK IIF satellites transmitting the L5 signal, leading to a limited contribution to the convergence time. Another reason may have been due to the satellites' DCBs being not corrected and more IFB parameters being estimated. However, the positioning accuracies of the static triple-frequency PPP or PPP AR were slightly worse than those of the static dual-frequency PPP or PPP AR. This may have been caused by PCO and PCV model errors, since the satellite L2 signals were used for the third frequency, L5; this needs to be further studied later. Another reason may have been attributed to the residual IFCB corrections error on the L5 phase observation. In

addition, the convergence time and positioning accuracy of static PPP and PPP AR based on IGU orbits were slightly worse than those based on IGF orbits. A summary of the results for static PPP and PPP AR is shown in Table 1.

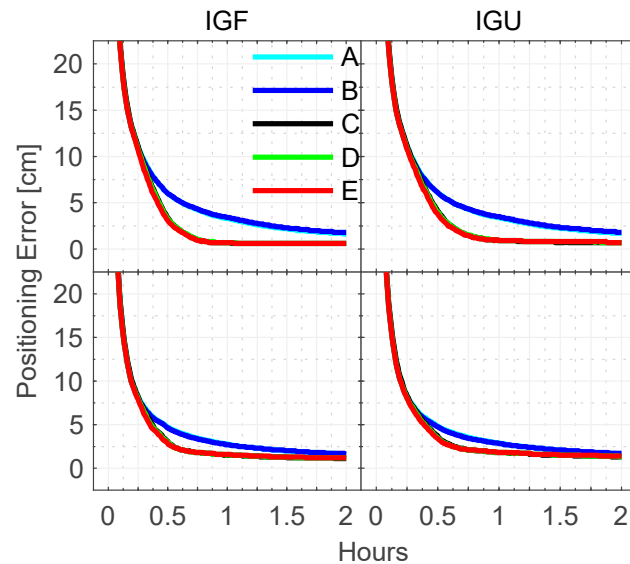


Figure 9. Convergence time analysis of the five groups of static 2 h PPP and PPP AR solutions for all the rovers from DOY 112 to 126, 2019: Top two panels represent the horizontal error; bottom two panels represent the vertical error.

3.2.2. Kinematic PPP

The average TTFFs and fixing rates of the three groups of kinematic PPP AR solutions based on IGF and IGU orbits over the 15 day period for every rover are presented in Figure 10. Average TTFFs of 36.0 and 43.9 min were achieved for Solution C based on IGF and IGU orbits, respectively, for all rovers, while average TTFFs of Solution D reached 34.6 and 42.2 min, respectively. Solution E achieved the fastest average TTFFs of 31.1 and 37.9 min, respectively. Compared to the static PPP AR, the kinematic PPP AR required longer TTFFs, mainly due to the relatively weak inter-epoch constraints on coordinates of kinematic PPP. However, more improvements were achieved for the kinematic triple-frequency PPP AR. With respect to the kinematic solutions of Solution C based on IGF and IGU orbits, improvements of 13.6% and 13.7%, respectively, were achieved for Solution E. In comparison, for the static solutions, the values were only 10.7% and 11.8%, respectively. In addition, with respect to the average TTFFs for the three groups of kinematic PPP AR based on IGF orbits, the average TTFFs for these based on IGU orbits were 21.9%, 22.0% and 21.9% longer, respectively.

Compared to the static PPP AR, the fixing rates were lower for the three groups of kinematic PPP AR. However, there was a small improvement in the fixing rates of the kinematic triple-frequency PPP AR over dual-frequency PPP AR solutions. Furthermore, the three groups of kinematic PPP AR based on IGU orbits had lower fixing rates than those based on IGF orbits. Average fixing rates of 97.0% and 95.6% were achieved for Solution C based on IGF and IGU orbits, respectively, for all rovers. The fixing rates increased slightly for Solutions D and E, and the highest fixing rate was achieved for Solution E. Average fixing rates of 97.1% and 95.8% were achieved for Solution D, respectively, while the average fixing rates reached 97.4% and 96.3% for Solution E, respectively.

Additionally, to evaluate the convergence times of the five groups of kinematic solutions, the PPP process was restarted every 2 h. Figure 11 presents the average position errors as a function of time since the start of PPP for all 15 stations from DOY 112 to 126, 2019. A total of 2475 independent kinematic PPP runs were performed for this analysis. Compared to static PPP and PPP AR, a longer convergence time was needed for kine-

matic PPP and PPP AR. The convergence time decreased substantially, and the positioning accuracy improved greatly for kinematic PPP AR compared to PPP. Furthermore, the introduction of the third frequency, L5, had a marginal impact on the convergence time and positioning accuracy of kinematic PPP and PPP AR. In addition, the convergence time and positioning accuracy of kinematic PPP and PPP AR based on IGU orbits were slightly worse than those based on IGF orbits. A summary of the results for kinematic PPP and PPP AR is shown in Table 2.

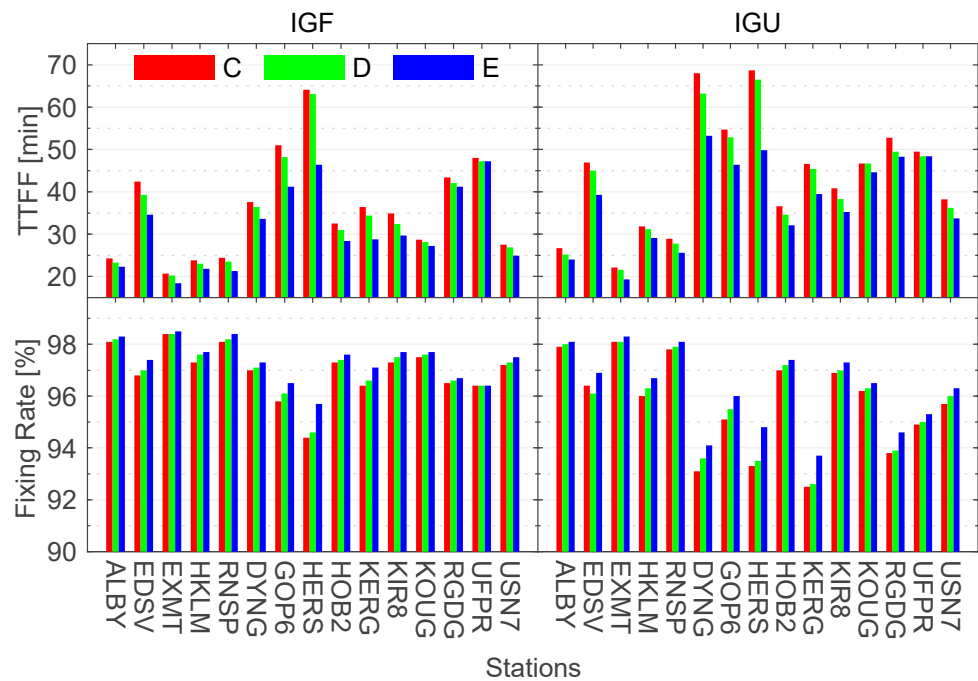


Figure 10. Average TTFFs and fixing rates of the three groups of kinematic 24 h PPP AR solutions for every rover from DOY 112 to 126, 2019.

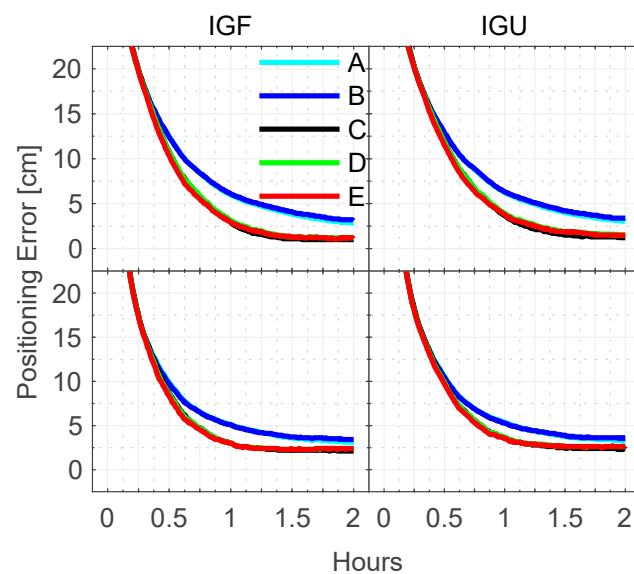


Figure 11. Convergence time analysis of the five groups of kinematic 2 h PPP and PPP AR solutions of all the rovers from DOY 112 to 126, 2019: top two panels represent the horizontal error; bottom two panels represent the vertical error.

4. Discussion

With respect to dual-frequency PPP AR, slight improvements in the TTFFs and fixing rates were achieved for GPS triple-frequency PPP AR, which may be attributed to the EWL ambiguities with long wavelengths, that could be quickly searched and fixed by introducing the third frequency, L5, in the ambiguities search stage. In addition, the introduction of the third frequency could also increase the number of candidate ambiguities, improving the passing rate of the ambiguity test. Furthermore, due to the smaller number of GPS satellites capable of transmitting the L5 signal, a marginal impact on the convergence time and positioning accuracy of PPP and PPP AR was achieved. This may also have resulted from the satellites' DCBs not being corrected, leading to more satellite- and receiver-dependent IFBs parameters being estimated.

Additionally, due to the relatively strong inter-epoch constraints on the coordinates of static PPP, longer TTFFs and lower fixing rates for kinematic PPP AR were achieved than static PPP AR. In contrast, compared to the improvements in the TTFFs and fixing rates for triple-frequency static PPP AR over dual-frequency static PPP AR, larger improvements were achieved for triple-frequency kinematic PPP AR than dual-frequency kinematic PPP AR. However, the positioning accuracies of static triple-frequency PPP or PPP AR were slightly worse than those of static dual-frequency PPP or PPP AR, which may have been due to the inaccurate phase center correction model for the third-frequency signal of receiver and satellite antennas. On the other hand, it may also have been caused by the residual IFCB correction errors on the L5 phase observations, which need to be further studied in future works.

We look forward to improving the GPS triple-frequency PPP AR performance with the elaboration of a phase center correction model for the third frequency signal of receiver and satellite antennas. In addition, the deployment of more BLOCK IIIA satellites capable of transmitting three frequency signals in the future is also expected to contribute to the improved performance of GPS triple-frequency PPP AR.

5. Conclusions

To investigate the impact of the IGU orbit errors on the GPS triple-frequency uncombined PPP AR performance, the EWL, WL and NL FCBs of GPS satellites were generated with the SD model using global reference stations based on the IGU orbits. They were compared with the EWL, WL and NL FCBs estimates based on IGF orbits in terms of precision and stability for the first time. The experimental results illustrate that the EWL, WL and NL FCBs generated based on IGF orbits were quite steady in a 1 day period. Due to the long wavelength of the EWL and WL ambiguities, the EWL and WL FCBs generated based on IGU orbits exhibited comparable precision and stability to those generated based on IGF orbits. In contrast, due to the short wavelength of the NL ambiguities, the precision and stability of NL FCBs were affected by the orbit errors assimilated into the L1 and L2 ambiguities, which were not compensated for by satellite clock error corrections. As a result, the NL FCBs generated based on the IGU orbits performed worse than those generated based on the IGF orbits.

Compared to PPP AR based on the IGF orbits, longer TTFFs and lower fixing rates were achieved for PPP AR based on the IGU orbits, which were attributed mainly to the impact of the IGU orbit errors, as well as the lower precision and poorer stability of the FCB estimates. Furthermore, the convergence time and positioning accuracy of PPP and PPP AR based on the IGU orbits were slightly worse than those based on the IGF orbits. Moreover, due to the relatively strong inter-epoch constraints on coordinates of static PPP and PPP AR, the impacts of the IGU orbit errors on the kinematic PPP and PPP AR were obviously larger than those on the static PPP and PPP AR. It is expected that the reliability and stability of real-time GPS triple-frequency PPP AR can be further enhanced with the improvement of the IGU orbit accuracy.

Author Contributions: Conceptualization, L.Q.; methodology, L.Q.; software, L.Q.; validation, L.Q. and P.Z.; formal analysis, L.Q.; investigation, P.Z.; resources, C.J.; data curation, C.J.; writing-original draft preparation, L.Q.; writing-review and editing, L.Q.; visualization, J.L.; supervision, J.W.; project administration, M.D.; funding acquisition, Q.Z. All authors have read and agreed to the published version of the manuscript.

Funding: This research was funded by Beijing Natural Science Foundation, Grant Number 4204094, General research project of Beijing education commission, Grant Number KM201910016007, National Key Research and Development Program of China, Grant Number 2018YFC0706003 and National Science Foundation (NSFC) of China, Grant Number 41874029 and 41930650.

Data Availability Statement: IGS orbit/clock products can be obtained from <ftp://igs.gnsswhu.cn/pub/gps/products/> (accessed on 1 June 2021), IGS observation data can be obtained from <ftp://igs.gnsswhu.cn/pub/gps/data/daily/2019/> (accessed on 1 June 2021).

Acknowledgments: The authors would like to thank the International GNSS service (IGS) for kindly providing the orbit/clock products and observation data. We are also grateful to the reviewers' valuable comments and suggestions. The use of Generic Mapping Tool (GMT) software is also acknowledged.

Conflicts of Interest: The authors declare no conflict of interest.

References

1. Li, T.; Wang, J.; Laurichesse, D. Modeling and quality control for reliable precise point positioning integer ambiguity resolution with GNSS modernization. *GPS Solut.* **2014**, *18*, 429–442. [[CrossRef](#)]
2. Geng, J.; Guo, J.; Chang, H.; Li, X. Toward global instantaneous decimeter-level positioning using tightly coupled multi-constellation and multi-frequency GNSS. *J. Geod.* **2018**, *93*, 977–991. [[CrossRef](#)]
3. Geng, J.; Guo, J.; Meng, X.; Gao, K. Speeding up PPP ambiguity resolution using triple-frequency GPS/BeiDou/Galileo/QZSS data. *J. Geod.* **2020**, *94*, 1–15. [[CrossRef](#)]
4. Ge, M.; Chen, J.; Douša, J.; Gendt, G.; Wickert, J. A computationally efficient approach for estimating high-rate satellite clock corrections in realtime. *GPS Solut.* **2012**, *16*, 9–17. [[CrossRef](#)]
5. Li, P.; Zhang, X.; Ren, X.; Zuo, X.; Pan, Y. Generating GPS satellite fractional cycle bias for ambiguity-fixed precise point positioning. *GPS Solut.* **2016**, *20*, 771–782. [[CrossRef](#)]
6. Geng, J.; Guo, J. Beyond three frequencies: An extendable model for single-epoch decimeter-level point positioning by exploiting Galileo and BeiDou-3 signals. *J. Geod.* **2020**, *94*, 1–15. [[CrossRef](#)]
7. Laurichesse, D.; Banville, S.; Innovation: Instantaneous Centimeter-level Multi-frequency Precise Point Positioning. GPS World 4 July 2018. Available online: <https://www.gpsworld.com/innovation-instantaneous-centimeter-level-multi-frequency-precise-point-positioning/> (accessed on 1 June 2021).
8. El-Mowafy, A.; Deo, M.; Kubo, N. Maintaining real-time precise point positioning during outages of orbit and clock corrections. *GPS Solut.* **2017**, *21*, 937–947. [[CrossRef](#)]
9. Douša, J. The impact of errors in predicted GPS orbits on zenith troposphere delay estimation. *GPS Solut.* **2010**, *14*, 229–239. [[CrossRef](#)]
10. Li, Y.; Gao, Y.; Li, B. An impact analysis of arc length on orbit prediction and clock estimation for PPP ambiguity resolution. *GPS Solut.* **2015**, *19*, 201–213. [[CrossRef](#)]
11. Li, Y.; Gao, Y.; Shi, J. Improved PPP ambiguity resolution by COES FCB estimation. *J. Geod.* **2016**, *90*, 437–450. [[CrossRef](#)]
12. Montenbruck, O.; Hugentobler, U.; Dach, R.; Steigenberger, P.; Hauschild, A. Apparent clock variations of the Block IIF-1 (SVN62) GPS satellite. *GPS Solut.* **2011**, *16*, 303–313. [[CrossRef](#)]
13. Xie, X.; Fang, R.; Geng, T.; Wang, G.; Zhao, Q.; Liu, J. Characterization of GNSS signals tracked by the iGMAS network considering recent BDS-3 satellites. *Remote Sens.* **2018**, *10*, 1736. [[CrossRef](#)]
14. Pan, L.; Zhang, X.; Guo, F.; Liu, J. GPS inter-frequency clock bias estimation for both uncombined and ionospheric-free combined triple-frequency precise point positioning. *J. Geod.* **2019**, *93*, 473–487. [[CrossRef](#)]
15. Odijk, D.; Zhang, B.; Khodabandeh, A.; Odolinski, R.; Teunissen, P.J.G. On the estimability of parameters in undifferenced, uncombined GNSS network and PPP-RTK user models by means of S-system theory. *J. Geod.* **2015**, *90*, 15–44. [[CrossRef](#)]
16. Qu, L.; Du, M.; Wang, J.; Gao, Y.; Zhao, Q.; Zhang, Q.; Guo, X. Precise point positioning ambiguity resolution by integrating BDS-3e into BDS-2 and GPS. *GPS Solut.* **2019**, *23*, 63. [[CrossRef](#)]
17. Guo, J.; Geng, J. GPS satellite clock determination in case of inter-frequency clock biases for triple-frequency precise point positioning. *J. Geod.* **2018**, *92*, 1133–1142. [[CrossRef](#)]
18. Montenbruck, O.; Hauschild, A.; Steigenberger, P.; Langley, R.B. Three's the challenge: A close look at GPS SVN62 triple-frequency signal combinations finds carrier-phase variations on the new L5. *GPS World* **2010**, *21*, 8–19.
19. Li, X.; Ge, M.; Zhang, H.; Wickert, J. A method for improving uncalibrated phase delay estimation and ambiguity-fixing in real-time precise point positioning. *J. Geod.* **2013**, *87*, 405–416. [[CrossRef](#)]

20. Teunissen, P.J.G. The least-squares ambiguity decorrelation adjustment: A method for fast GPS integer ambiguity estimation. *J. Geod.* **1995**, *70*, 65–82. [[CrossRef](#)]
21. Teunissen, P.J.G. Success probability of integer GPS ambiguity rounding and bootstrapping. *J. Geod.* **1998**, *72*, 606–612. [[CrossRef](#)]
22. Li, P.; Zhang, X.; Ge, M.; Schuh, H. Three-frequency BDS precise point positioning ambiguity resolution based on raw observables. *J. Geod.* **2018**, *92*, 1357–1369. [[CrossRef](#)]
23. Gao, W.; Gao, C.; Pan, S.; Wang, D.; Deng, J. Improving ambiguity resolution for medium baselines using combined GPS and BDS dual/triple-frequency observations. *Sensors* **2015**, *15*, 27525–27542. [[CrossRef](#)]
24. Johnston, G.; Riddell, A.; Hausler, G. *The International GNSS Service*. Teunissen, In *Handbook of Global Navigation Satellite Systems*, 1st ed.; Peter, J.G., Montenbruck, O., Eds.; Springer: Cham, Switzerland, 2017; pp. 967–982. [[CrossRef](#)]
25. Li, H.; Zhou, X.; Wu, B. Fast estimation and analysis of the inter-frequency clock bias for Block IIF satellites. *GPS Solut.* **2013**, *17*, 347–355. [[CrossRef](#)]
26. Gu, S.; Shi, C.; Lou, Y.; Liu, J. Ionospheric effects in uncalibrated phase delay estimation and ambiguity-fixed PPP based on raw observable model. *J. Geod.* **2015**, *89*, 447–457. [[CrossRef](#)]
27. Nandarajah, N.; Khodabandeh, A.; Wang, K.; Choudhury, M.; Teunissen, P.J.G. Multi-GNSS PPP-RTK: From Large- to Small-Scale Networks. *Sensors* **2018**, *18*, 1078. [[CrossRef](#)]
28. Hu, J.; Zhang, X.; Li, P.; Ma, F.; Pan, L. Multi-GNSS fractional cycle bias products generation for GNSS ambiguity-fixed PPP at Wuhan University. *GPS. Solut.* **2020**, *24*, 1–13. [[CrossRef](#)]
29. Liu, G.; Guo, F.; Wang, J.; Du, M.; Qu, L. Triple-frequency GPS un-differenced and uncombined PPP ambiguity resolution using observable-specific satellite signal biases. *Remote Sens.* **2020**, *12*, 2310. [[CrossRef](#)]